

# Solar parity issue with flux-transport dynamo

H. Hotta and T. Yokoyama

Department of Earth and Planetary Science, University of Tokyo, 7-3-1 Hongo, Bunkyo-ku,  
Tokyo 113-0033, Japan

[hotta.h@eps.s.u-tokyo.ac.jp](mailto:hotta.h@eps.s.u-tokyo.ac.jp)

Received \_\_\_\_\_; accepted \_\_\_\_\_

arXiv:1004.2088v1 [astro-ph.SR] 13 Apr 2010

## ABSTRACT

We investigated the dependence of the solar magnetic parity between the hemispheres on two important parameters, the turbulent diffusivity and the meridional flow, by means of axisymmetric kinematic dynamo simulations based on the flux-transport dynamo model. It is known that the coupling of the magnetic field between hemispheres due to turbulent diffusivity is an important factor for the solar parity issue, but the detailed criterion for the generation of the dipole field has not been investigated. Our conclusions are as follows. (1) The stronger diffusivity near the surface is more likely to cause the magnetic field to be a dipole. (2) The thinner layer of the strong diffusivity near the surface is also more apt to generate a dipolar magnetic field. (3) The faster meridional flow is more prone to cause the magnetic field to be a quadrupole, i.e., symmetric about the equator. These results show that turbulent diffusivity and meridional flow are crucial for the configuration of the solar global magnetic field.

*Subject headings:* Sun: activity — Sun: interior — Sun: dynamo

## 1. Introduction

The solar magnetic 11-year cycle is thought to be sustained by the dynamo motion of the internal ionized plasma (Parker 1955). Based on the internal structure of the velocity field, i.e., the meridional flow and the differential rotation revealed by helioseismology (see review by Thompson et al. 2003), the flux-transport dynamo was suggested (Choudhuri et al. 1995; Dikpati & Charbonneau 1999; Küker et al. 2001; Hotta & Yokoyama 2010), as a model to successfully explain some features of solar activity such as the equatorward migration of sunspots and the poleward migration of the surface field.

The solar global field has a distinct parity: the poloidal field is a dipole, i.e., antisymmetric about the equator. The polar fields almost always have the different sign between hemispheres, even though they show the occasional weak north-south asymmetry in phase and amplitude. In addition, Hale’s polarity law states that the sunspots between hemispheres are nearly always antisymmetric about the equator (Hale 1908). It can then be interpreted that the toroidal fields ( $B_\phi$ ) below the surface are antisymmetric about the equator. This interesting feature is, however, not axiomatically explained by the flux transport dynamo model since this model significantly depends on three free parameters, i.e., the  $\alpha$ -effect, the meridional flow, and the turbulent diffusivity.

It has been suggested that the  $\alpha$ -effect around the base of the convection zone leads to the generation of the global dipolar magnetic field. (Dikpati & Gilman 2001; Bonanno et al. 2002; Chatterjee et al. 2004). The existence of the poloidal fields around the tachocline and the coupling of these fields between hemispheres are significant factors for the generation of the dipole field. A detailed explanation of this process is given in the next paragraph. Chatterjee et al. (2004) also suggested, however, that the dipole field can be obtained with the strong diffusivity in the convection zone without the presence of the  $\alpha$ -effect around the tachocline. Hence the exact necessity of the  $\alpha$ -effect in generating the dipole field is still

inconclusive.

The dependence of the parity on these parameters can be explained when we understand the role of the turbulent diffusivity in the solar magnetic parity issue. If the global magnetic field is antisymmetric, i.e. is a dipole like our sun, the  $\phi$  component of the magnetic vector potential in each hemisphere has the same sign (Fig. 1a). When the cyclic phase in one hemisphere slightly differs from the other, the coupling effect by the turbulent diffusivity of the poloidal field distinguishes the phase difference in the vector potential and causes the magnetic field to be a dipole. On the other hand, when the magnetic field is symmetric, i.e., is a quadrupole, this effect does not occur. Therefore the substantial coupling of the poloidal field generates the antisymmetric (a dipole) magnetic field. The sign of the toroidal field in one hemisphere differs from that in the other hemisphere when the global magnetic field is a solar-like dipole. With the same logic posited above, it is obvious that the substantial diffusive coupling of the toroidal field between the hemispheres helps the magnetic field to become symmetric (a quadrupole; Fig 1b). In summary, the parity of the stellar global magnetic field depends on which field, the toroidal or the poloidal, is more coupled by the turbulent diffusivity between the hemispheres. Detailed systematic parameter studies are necessary to understand for the parity issue.

In this study, we investigate the dependence of the solar magnetic parity on the distribution of the turbulent diffusivity and the amplitude of the meridional flow. The obtained constraint on the turbulent diffusivity is important since it is one of the key components of the solar dynamo model, although it is difficult to measure by direct observations.

## 2. Model

We solve axisymmetric kinematic dynamo equations. The magnetic field is divided into the toroidal field  $B$  and the poloidal field  $\mathbf{B}_p = \nabla \times [A(r, \theta)\mathbf{e}_\phi]$  in the spherical coordinate  $(r, \theta, \phi)$  as

$$\mathbf{B} = B(r, \theta)\mathbf{e}_\phi + \mathbf{B}_p \quad (1)$$

where  $A$  is the  $\phi$  component of the magnetic vector potential and  $\mathbf{e}_\phi$  is the unit vector along the  $\phi$  direction. Then the following standard forms of the dynamo equation are derived from the magnetic induction equation as

$$\begin{aligned} \frac{\partial B}{\partial t} + \frac{1}{r} \left[ \frac{\partial}{\partial r}(ru_r B) + \frac{\partial}{\partial \theta}(u_\theta B) \right] \\ = r \sin \theta (\mathbf{B}_p \cdot \nabla) \Omega - (\nabla \eta \times \nabla \times B \mathbf{e}_\phi) \cdot \mathbf{e}_\phi \end{aligned} \quad (2)$$

$$\begin{aligned} + \eta \left( \nabla^2 - \frac{1}{r^2 \sin^2 \theta} \right) B, \\ \frac{\partial A}{\partial t} + \frac{1}{r \sin \theta} (\mathbf{u} \cdot \nabla)(r \sin \theta A) \\ = \eta \left( \nabla^2 - \frac{1}{r^2 \sin^2 \theta} \right) A + S(r, \theta; B). \end{aligned} \quad (3)$$

We specify the meridional flow  $\mathbf{u} = u_r \mathbf{e}_r + u_\theta \mathbf{e}_\theta$ , the differential rotation  $\Omega$ , and the turbulent diffusivity  $\eta$ . A source term  $S(r, \theta; B)$  is artificially added to the right-hand side of equation (3). This source term describes the generation of poloidal fields at the solar surface from the decay of bipolar sunspots. This is the ‘‘Babcock-Leighton  $\alpha$ -effect’’ (Leighton 1969; Babcock 1961). Once these quantities are specified, we can solve equations (2) and (3) to study the behavior of the dynamo kinematically.

The formula for the differential rotation is given as

$$\Omega(r, \theta) = \Omega_c + \frac{1}{2} \left[ 1 + \operatorname{erf} \left( 2 \frac{r - r_c}{d_c} \right) \right] \{ \Omega_s(\theta) - \Omega_c \} \quad (4)$$

where  $\Omega_s(\theta) = \Omega_{\text{Eq}} + a_2 \cos^2 \theta + a_4 \cos^4 \theta$  is the surface latitudinal differential rotation and  $\operatorname{erf}$  is the error function. The parameters are set as  $\Omega_c/2\pi = 432.8$  nHz,  $\Omega_{\text{Eq}}/2\pi = 460.7$  nHz,

$a_2/2\pi = -62.69$  nHz,  $a_4/2\pi = -67.13$  nHz, and  $r_c = 0.7R$  and  $d_c = 0.05R$ , which closely resemble the best-fit helioseismic solution.  $R$  is the solar radius.  $r_c$  and  $d_c$  is the central radius and the thickness of the tachocline, respectively.  $\Omega_c$  is the rotating rate of the core. This differential rotation profile has a purely latitudinal difference with equatorial acceleration in the convection zone. It smoothly matches across the “tachocline” with the core rotating rigidly.

We now describe how the meridional flow is specified. While a poleward meridional flow is observed near the solar surface, the structure of the internal return flow is at present unconstrained observationally. We choose here an analytical form suggested by van Ballegooijen & Choudhuri (1988) with the density profile in the convection zone given by  $\rho(r) \propto [(R/r) - 1]^m$ ; the  $r$  and  $\theta$  components of this flow are as follows:

$$u_r(r, \theta) = \frac{u_0}{f} \left( \frac{R}{r} \right)^2 \times \left[ -\frac{1}{m+1} + \frac{c_1}{2m+1} \xi^m - \frac{c_2}{2m+p+1} \xi^{m+p} \right] \times \xi \sin^q \theta [(q+2) \cos^2 \theta - \sin^2 \theta] \quad (5)$$

$$u_\theta(r, \theta) = \frac{u_0}{f} \left( \frac{R}{r} \right)^3 [-1 + c_1 \xi^m - c_2 \xi^{m+p}] \times \sin^{q+1} \theta \cos \theta, \quad (6)$$

where

$$\xi(r) = \frac{R}{r} - 1, \quad (7)$$

$$c_1 = \frac{(2m+1)(m+p)}{(m+1)p} \xi_p^{-m}, \quad (8)$$

$$c_2 = \frac{(2m+p+1)m}{(m+1)p} \xi_p^{-(m+p)}, \quad (9)$$

$$\xi_p = \frac{R}{r_p} - 1. \quad (10)$$

As shown in eqs. (5) and (6),  $u_0$  is the amplitude of the velocity and  $p$  and  $q$  are respectively the radial and latitudinal dependence of the flow. We specify the bottom of the meridional flow  $r_p$ , and the normalization constant  $f$  to set the maximum speed of the meridional flow of the  $\theta$  component to  $u_0$ . We use the parameter values  $m = 0.5$ ,  $p = 0.25$ ,  $q = 0$  and  $r_p = 0.62R$ . Note that our meridional flow slightly penetrates into the rigidly rotating core, i.e.  $r_p < r_c$  (Hotta & Yokoyama 2010).

We assume that the net magnetic diffusivity in the convection zone is dominated by its turbulent contribution. We adopt a diffusivity profile of the form

$$\begin{aligned} \eta(r) = & \eta_{\text{core}} + \frac{\eta_t}{2} \left[ 1 + \operatorname{erf} \left( \frac{r - r_1}{d_1} \right) \right] \\ & + \frac{\eta_s}{2} \left[ 1 + \operatorname{erf} \left( \frac{r - r_2}{d_2} \right) \right]. \end{aligned} \quad (11)$$

Here,  $r_1 = 0.7R$ ,  $d_1 = 0.02R$  and  $d_2 = 0.02R$ . This profile consists of three layers. In the strong diffusivity layer ( $r > r_2$ ), the diffusivity is prescribed by  $\eta_s$  within  $10^{12} - 10^{14} \text{ cm}^2 \text{ s}^{-1}$ . Wang et al. (1989) argued that the surface diffusivity should be  $6 \times 10^{12} \text{ cm}^2 \text{ s}^{-1}$  to be consistent with observations of the time development of the surface magnetic field. In the convection zone we use the fixed value  $\eta_t = 5 \times 10^{10} \text{ cm}^2 \text{ s}^{-1}$ . In the subadiabatically stratified core there is no turbulence (or at least, far less), so that the diffusivity is presumably much weaker. We use the value  $\eta_{\text{core}} = 5 \times 10^8 \text{ cm}^2 \text{ s}^{-1}$ . For convenience, we define the surface depth  $d_s = R - r_2$  which denotes the thickness of the strong diffusivity layer. We take  $d_s$  and  $\eta_s$  as free parameters, since they affect the parity of the magnetic field.

Some parts of the toroidal field in the tachocline rise to the surface due to the magnetic buoyancy and generate active regions. During this process, the flux tube expands and the Coriolis force bends the flux. There is observational evidence offered by Babcock (1959) that the decay of tilted bipolar active regions can produce a substantial amount of the net poloidal fields near the surface (Wang & Sheeley 1991). This is called the

“Babcock-Leighton  $\alpha$ -effect.” Based on this, we assume that the poloidal source term is taken in the form

$$S(r, \theta; B) = \alpha(r, \theta) B(r_c, \theta) \times \left[ \frac{1}{1 + (B(r_c, \theta)/B_{\text{eq}})^2} \right], \quad (12)$$

where

$$\alpha(r, \theta) = \frac{s_0}{4} \times \left[ 1 + \operatorname{erf} \left( \frac{r - r_4}{d_4} \right) \right] \left[ 1 - \operatorname{erf} \left( \frac{r - r_5}{d_5} \right) \right] \times \sin \theta \cos \theta \left[ \frac{1}{1 + e^{-\gamma(\theta - \pi/4)}} \right]. \quad (13)$$

The parameters are  $r_4 = 0.95R$ ,  $r_5 = R$ ,  $d_4 = 0.05R$ ,  $d_5 = 0.01R$ , and  $\gamma = 30$ . We concentrate the  $\alpha$ -effect by the last factor in eq. (13) at the low latitude in which there are many observed active regions (Dikpati et al. 2004). The source term is made proportional to the toroidal field strength at the same latitude in the tachocline  $r = r_c$  (eq. (4)), i.e. the base of the convection zone, since it is assumed here to originate from the radially emerged magnetic fluxes. The quenching term  $\{1 + [B(r_c, \theta)/B_{\text{eq}}]^2\}^{-1}$  in eq. (12) ensures that the poloidal field production rapidly vanishes as the deep toroidal field strength exceeds  $B_{\text{eq}}$  (Cattaneo & Hughes 1996).  $B_{\text{eq}}$  is the equipartition magnetic field. The Coriolis force cannot bend a strong magnetic field ( $> B_{\text{eq}}$ ) in the convection zone. We use a fixed value  $B_{\text{eq}} = 4 \times 10^4$  G.  $s_0$  is determined by fixing the value of the dynamo number (see §3 in detail).

We solve equations (2) and (3) numerically in all the sphere of the meridional plane in  $0.6R < r < R$  and  $0 < \theta < \pi$  with the modified Lax-Wendroff scheme. We use a moderate resolution of around 64 grid points in the radial direction and 128 grid points in the latitudinal direction. At the lower boundary ( $r = 0.6R$ ), we set both  $B$  and  $A$  at zero, indicating that the radiative core is a perfect conductor. At the top boundary



( $r = R$ ), we set  $B = 0$  and smoothly match  $A$  onto an exterior potential field solution (Dikpati & Choudhuri 1994). At both poles ( $\theta = 0$  and  $\pi$ ), we set  $B = A = 0$  for the regularity. The numerical convergence is checked by runs with different grid spacings.

### 3. Results

A new indicator of the magnetic parity is defined in this study. The radial magnetic field at the surface can be decomposed as

$$B_r(R, \theta) = \sum_{n=0} c_n P_n(\cos \theta), \quad (14)$$

where  $P_n$  is the Legendre polynomial. Then we define the symmetric parameter as

$$\text{SP} = \frac{\sum_{i=0} |c_{2i}| - \sum_{i=0} |c_{2i+1}|}{\sum_{i=0} |c_i|}. \quad (15)$$

Each even (odd) order of the Legendre polynomial is symmetric (antisymmetric) about the equator. Therefore,  $\text{SP} = 1$  corresponds to the purely symmetric mode about the equator and  $\text{SP} = -1$  is the antisymmetric mode.

We first show a representative reference solution, computed with the amplitude of the meridional flow  $u_0 = 1000 \text{ cm s}^{-1}$ , the amplitude of the  $\alpha$ -effect  $s_0 = 160 \text{ cm s}^{-1}$ , the amplitude of the turbulent diffusivity near the surface layer  $\eta_s = 2 \times 10^{12} \text{ cm}^2 \text{ s}^{-1}$  and the thickness of the strong diffusivity layer  $d_s = 0.1R$ . The results are shown in the time-latitude plots in Fig. 2. This simulation is started with a symmetric initial condition. As time passes, the global magnetic field becomes antisymmetric. In such a case, the symmetric parameter develops as shown in Fig. 3. The black (red) line denotes the result with a symmetric (antisymmetric) initial condition. Regardless of the initial condition, the parity of the magnetic field approaches the stationary antisymmetric state where the

symmetric parameter becomes  $\sim -1$ . We conclude that the magnetic field with these reference parameters finally becomes a dipole field.

We investigate the asymptotic stationary values of the symmetric parameter for runs in different setups. We carried out runs by choosing a value for the surface diffusivity  $\eta_s$ , from 8 points in the range  $6 \times 10^{11}$  to  $1 \times 10^{13}$   $\text{cm}^2 \text{s}^{-1}$  and the surface depth  $d_s$ , from 5 points in the range  $0.1R$  to  $0.25R$ . We specify the amplitude of the  $\alpha$ -effect by

$$s_0 = 160 \text{ cm s}^{-1} \left( \frac{\eta_s}{2 \times 10^{12} \text{ cm}^2 \text{ s}^{-1}} \right)^2 \left( \frac{d_s}{0.1R} \right)^2 \quad (16)$$

The background reason for this setup is to fix the value of the surface integrated dynamo number,

$$N_D = \frac{s_0 k_x R d_\alpha}{\eta_s^2 d_s^2 k^4} \frac{d}{dr} (r \Omega \sin \theta), \quad (17)$$

where  $k_x$  and  $k$  denote the wavenumber of the magnetic field and  $d_\alpha$  denotes the thickness of the layer where the  $\alpha$ -effect is effective, and where  $k_x$ ,  $k$  and  $d_\alpha$  are assumed to be unchanged from case to case. This dynamo number is kept unchanged since it determines the oscillatory nature of the dynamo. The reason for this idea is because the strong  $\alpha$ -effect is necessary to endure the diffusivity in the large area. We also vary the amplitude of the meridional flow:  $u_0 = 1000 \text{ cm s}^{-1}$  (slow meridional flow case) and  $2000 \text{ cm s}^{-1}$  (fast meridional flow case). For every parameter set, we conducted runs with both symmetric and antisymmetric initial conditions to ensure that the asymptotic value of the symmetric parameter does not depend on the initial parity.  $8(\text{diffusivity}) \times 4(\text{surface depth}) \times 2(\text{meridional flow}) \times 2(\text{initial parity}) = 128$  simulation runs carried out. All simulations are calculated for more than 10000 years.

There are two types of solutions when the value of the SP is around zero and we categorize them as “mixed-parity” cases. One type is similar to the reference case (Fig. 4a). The value of the SP finally converges. The other type is interesting in that the value

of the symmetric parameter does not converge and continues to oscillate between the quadrupole and the dipole solutions (Fig. 4b). Since the averaged value in the calculation duration is close to zero, we adopted it for the SP in such cases.

The results of this parameter space study are shown in Fig. 5. The dynamo cycle period is also shown by the contour lines. The period is shorter when the surface depth is thicker since the transport of the magnetic flux by the diffusivity is more effective. Panel (a) shows the result of the slow meridional flow case ( $u_0 = 1000 \text{ cm s}^{-1}$ ). Two points can be ascertained from this figure. One is that regardless of the surface depth, the strong diffusivity ( $> 3 \times 10^{12} \text{ cm}^2 \text{ s}^{-1}$ ) can make the magnetic field to become a dipole ( $\text{SP} \sim -1$ ). The other is that with the thinner surface depth, no strong diffusivity ( $> 1 \times 10^{12} \text{ cm}^2 \text{ s}^{-1}$ ) is needed to generate the dipole field. This means that the magnetic field is more likely to be a dipole with the thinner surface depth. Fig. 4b shows the result of the fast meridional flow case ( $u_0 = 2000 \text{ cm s}^{-1}$ ). It is obvious that the parameter area for the symmetric solutions, i.e.  $S_p > 0$ , increases. This indicates that the fast meridional flow causes the magnetic field to be symmetric.

#### 4. Discussion and Conclusion

We investigated the dependence of the global magnetic parity on the distribution of the diffusivity (the amplitude and the surface depth) and the amplitude of the meridional flow. Three results were obtained. First, the model shows that the stronger diffusivity near the surface acts to make the magnetic field a dipole. The diffusivity near the surface enhances mainly the coupling of the poloidal field near the surface between the hemispheres, leading to the generation of dipolar magnetic field. The second result is that the thinner layer of the strong surface diffusivity also works to cause the magnetic field to become dipolar. The thinner surface depth suppresses the coupling of the toroidal field between the hemispheres

since most of the toroidal field exists around the tachocline. The third result is that the fast meridional flow causes the magnetic field to become a quadrupole. The fast meridional flow prevents the poloidal field from coupling near the surface of the equator because the flow transports the poloidal field poleward. In addition, the flow transports the toroidal field around the tachocline equatorward, thus causing the coupling of the toroidal field. These three results quantitatively constrain the distribution and the amplitude of turbulent diffusivity, which cannot be determined by observation and is an important factor for the dynamo problem.

In this study, we did not investigate the dependence of the parity on the  $\alpha$ -effect in the convection zone, which may be a strong factor in causing the magnetic field to become a dipole. The poloidal field generated by this effect around the tachocline is transported equatorward by the meridional flow, and this process enhances the coupling of the poloidal field between the hemispheres (Dikpati & Gilman 2001; Bonanno et al. 2002; Chatterjee et al. 2004). It is possible that the criterion for a dipole field we obtain in this study may be modified with this type of  $\alpha$ -effect. We will discuss the possibility of the existence and the influence of the  $\alpha$ -effect in a forthcoming paper. Another interesting issue to be addressed is the possibility that the variation of the velocity field in the solar cycle affects the parity. In the calculations for the earth dynamo there is the significant difference between the kinematic and the MHD cases in the parity issue (Nishikawa & Kusano 2008). Thus, in the future we will investigate the parity issue with the Lorentz feedback (Rempel 2006).

Numerical computations were carried out on the general-purpose PC farm at the Center for Computational Astrophysics (CfCA) of the National Astronomical Observatory of Japan. The page charge for this paper is supported by CfCA. We have greatly benefited from the proofreading/editing assistance from the GCOE program.

## REFERENCES

- Babcock, H. D. 1959, *ApJ*, 130, 364
- Babcock, H. W. 1961, *ApJ*, 133, 572
- Bonanno, A., Elstner, D., Rüdiger, G., & Belvedere, G. 2002, *A&A*, 390, 673
- Cattaneo, F., & Hughes, D. W. 1996, *Phys. Rev. E*, 54, R4532
- Chatterjee, P., Nandy, D., & Choudhuri, A. R. 2004, *A&A*, 427, 1019
- Choudhuri, A. R., Schussler, M., & Dikpati, M. 1995, *A&A*, 303, L29+
- Dikpati, M., & Charbonneau, P. 1999, *ApJ*, 518, 508
- Dikpati, M., & Choudhuri, A. R. 1994, *A&A*, 291, 975
- Dikpati, M., de Toma, G., Gilman, P. A., Arge, C. N., & White, O. R. 2004, *ApJ*, 601, 1136
- Dikpati, M., & Gilman, P. A. 2001, *ApJ*, 559, 428
- Hale, G. E. 1908, *ApJ*, 28, 315
- Hotta, H., & Yokoyama, T. 2010, *ApJ*, 709, 1009
- Küker, M., Rüdiger, G., & Schultz, M. 2001, *A&A*, 374, 301
- Leighton, R. B. 1969, *ApJ*, 156, 1
- Nishikawa, N., & Kusano, K. 2008, *Physics of Plasmas*, 15, 082903
- Parker, E. N. 1955, *ApJ*, 122, 293
- Rempel, M. 2006, *ApJ*, 647, 662

Thompson, M. J., Christensen-Dalsgaard, J., Miesch, M. S., & Toomre, J. 2003, *ARA&A*, 41, 599

van Ballegooijen, A. A., & Choudhuri, A. R. 1988, *ApJ*, 333, 965

Wang, Y., Nash, A. G., & Sheeley, Jr., N. R. 1989, *ApJ*, 347, 529

Wang, Y., & Sheeley, Jr., N. R. 1991, *ApJ*, 375, 761

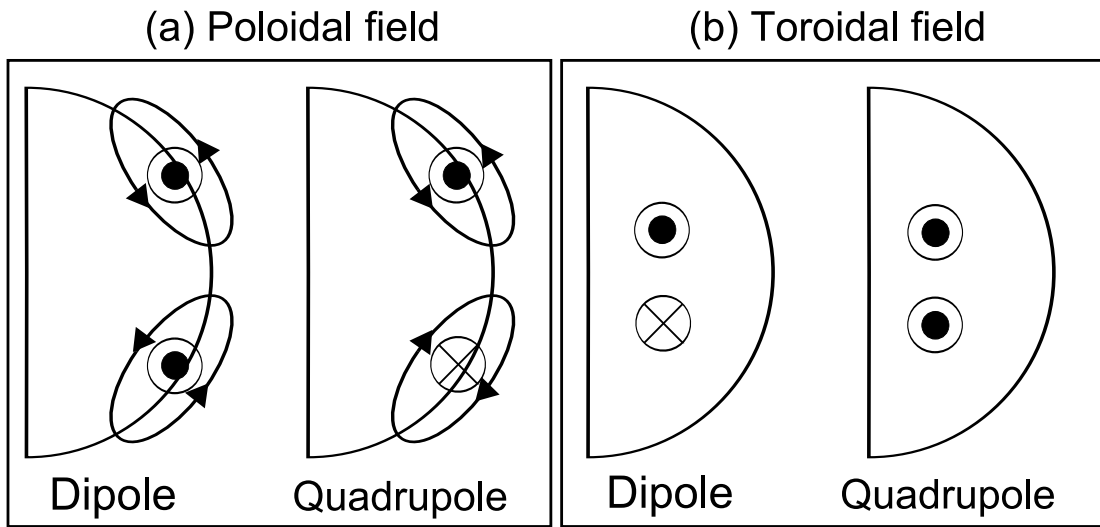


Fig. 1.— Illustration of the parity issue. Panel (a) shows the poloidal fields (line) for a dipole and a quadrupole field and the corresponding vector potentials. Panel (b) shows the toroidal field for a dipole and a quadrupole.

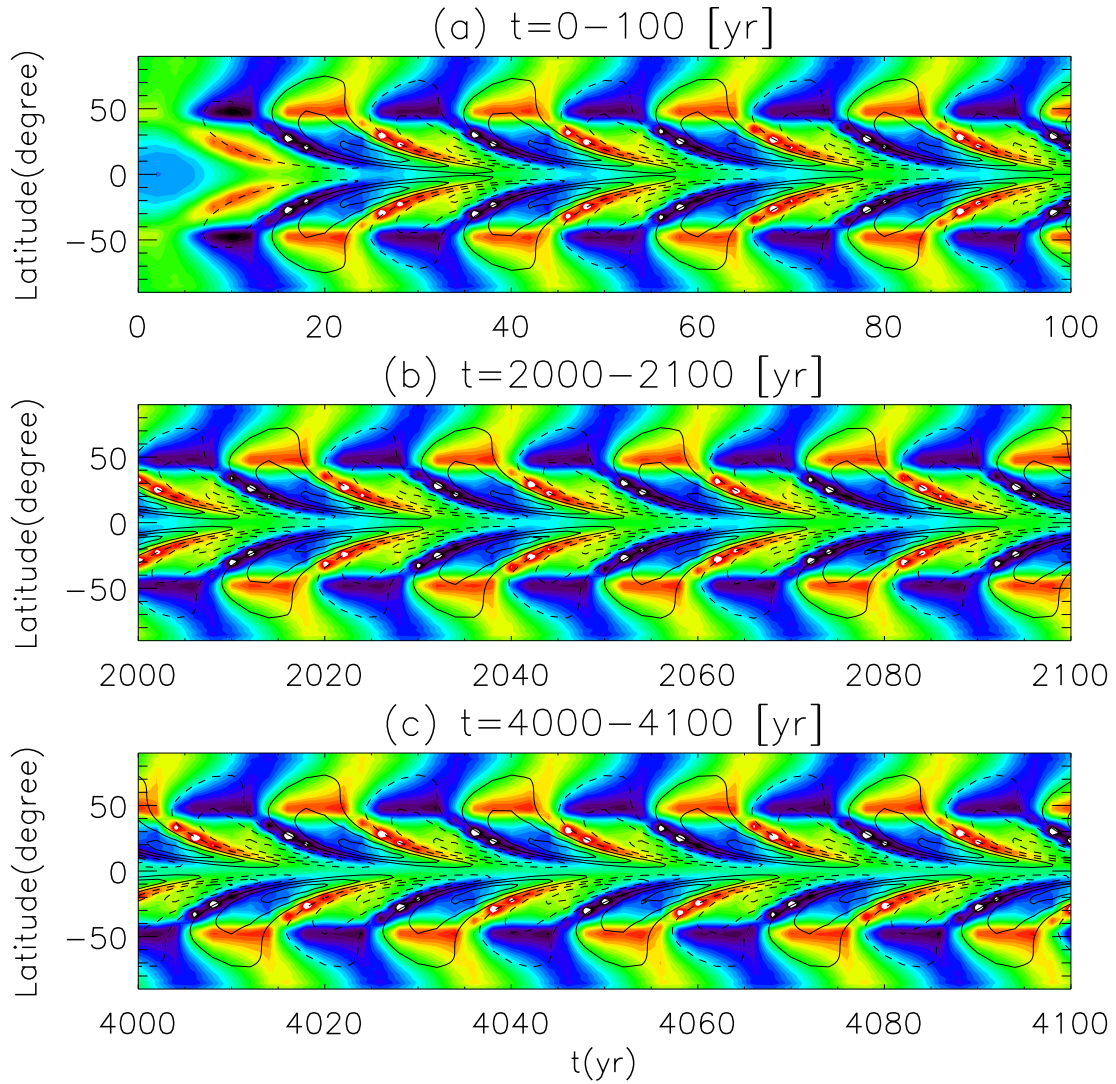


Fig. 2.— Butterfly diagram for the reference solution. Time-latitude plot of  $B_\phi|_{r=0.7R}$  by contour is superposed on the color map of the surface radial fields.



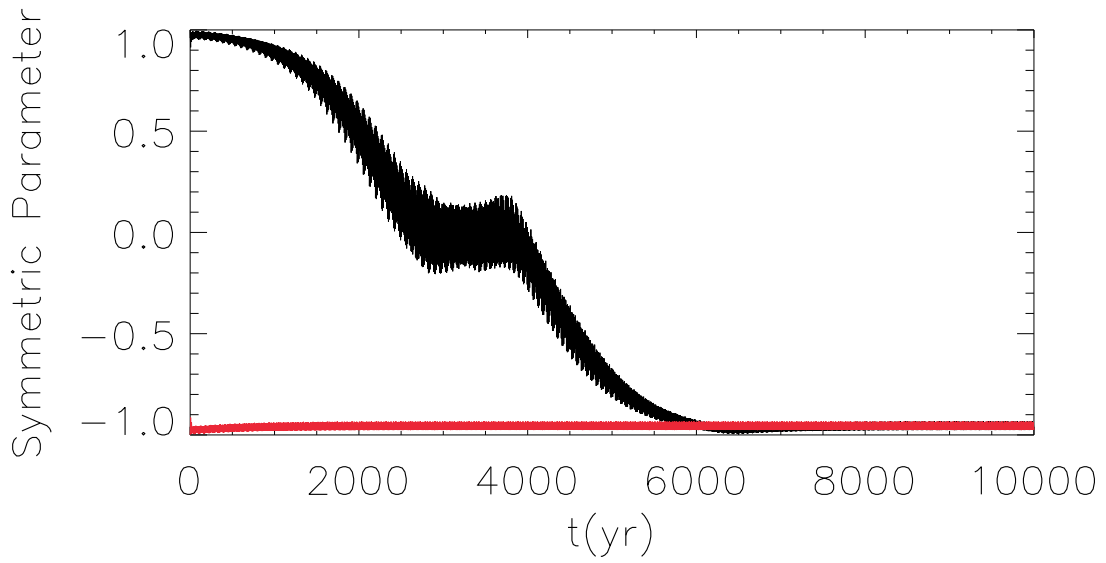


Fig. 3.— Time-development of the symmetric parameters. The black (red) line corresponds to the results of the symmetric (antisymmetric) initial condition. Regardless of the initial condition the symmetric parameter finally becomes  $\sim -1$  (antisymmetric solution).

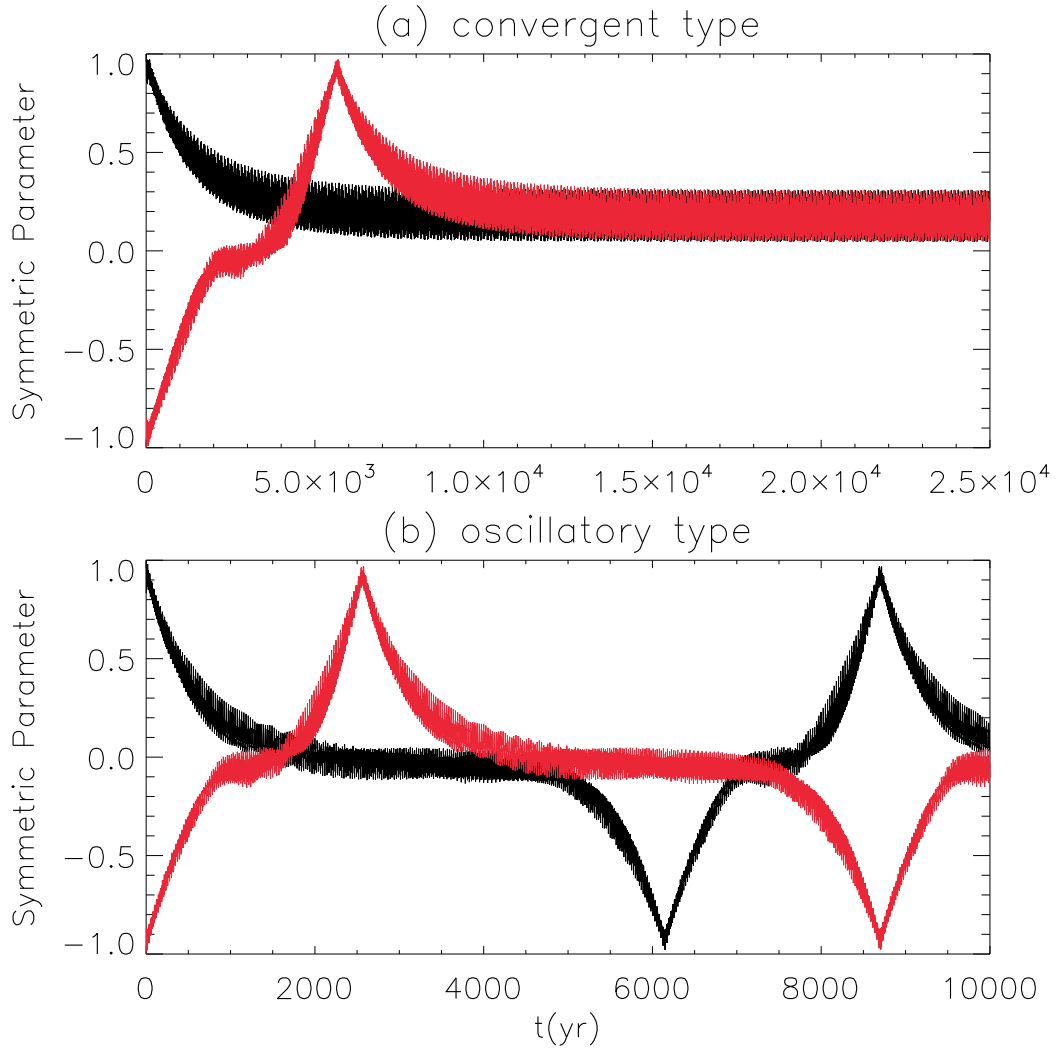


Fig. 4.— Two types in "zero" symmetric parameter cases. The time-development of the symmetric parameter for each type is shown. The format is the same as in Fig. 3. Panel (a) shows the convergent type in which the value of the symmetric parameter finally converges to zero. Panel (b) shows the oscillation type in which the symmetric parameter continues to oscillate between the quadrupole ( $SP \sim -1$ ) and the dipole ( $SP \sim 1$ ) solutions.

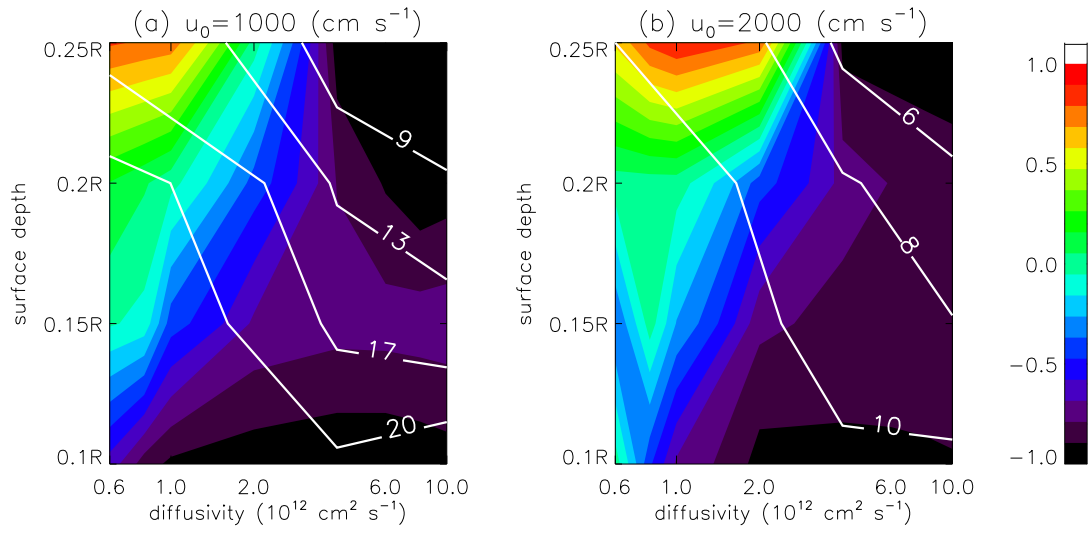


Fig. 5.— Symmetric parameter SP as a function of the diffusivity  $\eta_s$  and the surface depth  $d_s$ . The superposed lines indicate the contours of the dynamo cycle period over periods of years. Panel (a) shows the results for the slow meridional flow case ( $u_0 = 1000 \text{ cm s}^{-1}$ ). Panel (b) shows the result for the fast meridional flow case ( $u_0 = 2000 \text{ cm s}^{-1}$ ).